Materials & Design 227 (2023) 111745

Contents lists available at ScienceDirect

Materials & Design

journal homepage: www.elsevier.com/locate/matdes

Identifying damage mechanisms of composites by acoustic emission and supervised machine learning

Renato S.M. Almeida [a,*], Marcelo D. Magalhães [a,b], Md Nurul Karim [a], Kamen Tushtev [a,*], Kurosch Rezwan [a,c]

[a] Advanced Ceramics, University of Bremen, Bremen 28359, Germany
[b] Department of Mechanical Engineering, Federal University of Santa Catarina, Florianópolis, Brazil
[c] MAPEX - Center for Materials and Processes, University of Bremen, Bremen 28359, Germany

HIGHLIGHTS

- Experiments are conceptualized to collect specific acoustic emission signals of different damage mechanisms by evaluating composite constituents separately.
- The collected dataset is used to train a supervised machine learning classification model with accuracy of up to 88%
- Signals of a composite tensile test are classified giving information regarding location, time, frequency and intensity of each damage type.
- This approach can be applied to other materials to build a library containing characteristic features of different damage mechanisms.

GRAPHICAL ABSTRACT

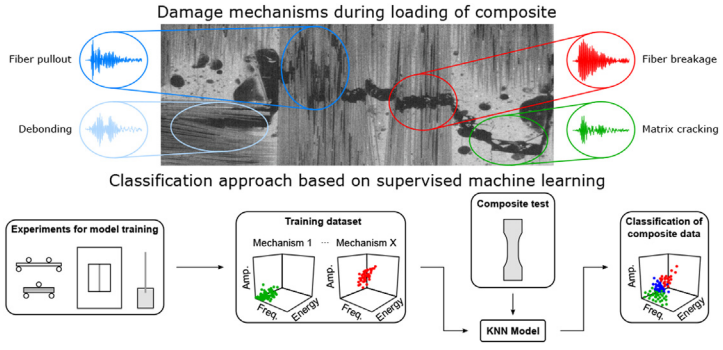

ARTICLE INFO

Article history:
Received 1 December 2022
Revised 1 February 2023
Accepted 13 February 2023
Available online 14 February 2023

Keywords:
Acoustic emission
Damage mechanisms
Supervised classification
Structural health monitoring
Ceramic matrix composites

ABSTRACT

Acoustic emission (AE) is a well-established technique for in-situ damage analysis of composite materials. The main challenge, however, is to be able to correlate the measured AE signals with their respective damage mechanism sources. Hence, an innovative approach to classify AE signals based on supervised machine learning is presented in this work. At first, the constituents of a composite (fiber, matrix and interface) are characterized separately and fingerprint information regarding the characteristic AE features of each damage mechanism is gathered. This dataset is then used to train a model based on the k-nearest neighbors algorithm. Model accuracy is calculated to be 88%. Subsequently, AE signals measured during tensile tests of commercial composites are classified by the trained model. The analysis provides important information regarding location, time, frequency and intensity of each damage mechanism. Matrix cracking and fiber debonding are the most frequent damage mechanisms representing around 40% and 20% of the measured AE hits. Nevertheless, fiber breakage is the mechanism that dissipates the most AE energy (40%) for the studied composite. Furthermore, the presented method can also be applied together with other techniques like computer tomography, delivering a powerful approach to understand different multi-phase materials.

* Corresponding authors.
E-mail addresses: renato.almeida@uni-bremen.de (R.S.M. Almeida), tushtev@uni-bremen.de (K. Tushtev).

https://doi.org/10.1016/j.matdes.2023.111745
0264-1275/

1. Introduction

Combining two or more materials to obtain distinct properties is the main goal of composite materials. This has been traditionally done for mechanical applications, in which fibers, whiskers, particles or even material layers are used to reinforce another material. The purpose of the reinforcement depends on the type of matrix to be reinforced [1]. Reinforcing polymers and metals increases their strength, while reinforcing ceramics increases their inherent low fracture toughness. In all cases, the final mechanical properties of the composites will depend on the properties of the constituents, how the mechanical load is distributed and how possible cracks propagate through the constituents. Naturally, the concept of composite materials has evolved over the years. Different materials are now combined to obtain unique properties not only related to mechanical performance. Hence, composites are now seen in several fields of material science such as biological-inspired composites [2] or composite materials for electronic [3] and optical [4] applications. The main common point of these composite materials is that their advanced properties are achieved by their complex, hierarchical and/or hybrid microstructures. Nevertheless, their complexity also makes them more difficult to be safely used. Mechanical and/or thermal loads, as well as the surrounding atmosphere, can damage the more sensitive constituents of a composite causing them to crack during their application. Thus, it is extremely important to detect such damage as it can potentially lead to the premature failure of the whole composite component in service.

Health monitoring and in-situ damage analysis of composites can be performed using non-destructive techniques like computer tomography (CT), microscopy, infrared thermography, measurement of electrical resistance or acoustic emission monitoring (AE) [5–12]; although each method has advantages and disadvantages. For instance, most conventional CT equipments do not have enough resolution to detect sharp cracks [6]. Microscopes can have much higher resolution, but the analysis is only 2D, while the damage can be in different planes. Furthermore, both of these imaging techniques have a compromise between resolution and field of view [6]. Among the other aforementioned methods, AE is a very interesting tool since it can detect the exact time that damage takes place, even from damage sources on the nanometer scale [13]. This technique consists of monitoring acoustic waves that are generated by the release of accumulated energy when microstructural changes like cracking happen [14]. Hence, AE signals contain key information on the damage source, but this information is very hard to decode. In fact, the main challenge of AE analysis is to be able to relate the measured signals with their responsible damage mechanism sources [14,15] since multiphase materials may show multiple damage mechanisms. Hence, the ability to properly categorize AE signals is the key to considerably improve health monitoring of complex materials.

In this matter, machine learning has been commonly used to classify AE signals [14]. Most of the works in this topic rely on clustering of AE signals by unsupervised pattern recognition approaches. For that, features that describe the AE signals are compared using a variety of identification codes and similar signals are grouped together [16–19]. Still, the main challenge of relating the different groups with their respective origins remains, not to mention that knowing the number of possible clusters is a problem of its own [14]. There are a few approaches to "handle" this issue, which normally involve the use of other in-situ observations like CT and microscopy [11,20–22] or the simulation of AE patterns [23,24]. Nevertheless, these associations can be rather speculative. A more direct identification can be made by supervised classification [21]. In this case, the data is classified by comparing with previously classified data, i.e., a training dataset. However, this raises another challenge since information regarding cracking of each constituent of a composite is normally not easily obtainable [14]. For instance, Gutkin et al. [17] characterized carbon fiber reinforced plastic composites under various test configurations to promote different types of damage. Nevertheless, since multiple damage mechanisms occur at the same time during the different loadings, a direct classification of the signals was not possible. Saeedifar et al. [25] used supervised classification to identify which material fails during the testing of composite-metal joints. Still, the classification of the different damage mechanisms was not possible since each material of the joint show multiple damage modes. Hence, methods to obtain a reliable training dataset to be used for supervised classification of damage modes within a composite material are presented in this work. The approach consists of testing each constituent of the composite individually to promote specific damage mechanisms and obtain their AE characteristics. This approach allows the correct identification of damage mechanisms during loading of composites. Consequently, this method can be used to understand damage development under operando conditions and better conceptualize composite materials for safe use in service.

2. Methods

2.1. Materials

The material evaluated in this work is a ceramic matrix composite (CMC) provided by the company Pritzkow Spezialkeramik (Filderstadt, Germany): FW12 composite containing Nextel 610 DF-11 fiber fabrics reinforcing an 85% Al_2O_3 + 15% 3YSZ matrix. The manufacturing of the composite was done by slurry infiltration. For that, a water-based slurry with organic binders was prepared. The fiber fabrics were infiltrated via knife blade coating and, subsequently, stacked and pressed together. The green plate was then dried and later sintered at 1200 °C. According to the manufacturer, this composite has a fiber content of approximately 40 vol% and porosity of about 33% [26]. An example photo and microstructure of the studied material showing the fiber reinforcement directions can be seen Fig. 1(a) and (b), respectively. This type of composite was chosen to demonstrate the classification approach since its complex microstructure leads to a material that shows, at the same time, high strength, thermal stability and damage tolerance. The enhanced damage tolerance is achieved by carefully adjusting the microstructure to promote crack deflection during loading [27]. In other words, it is essential that the cracks, which initiate in the matrix, should not penetrate into the fibers, but be instead deflected to dissipate mechanical energy. Ideally, the following damage mechanisms should take place before the total failure of the composite: matrix cracking, fiber–matrix debonding, fiber breakage and fiber pullout [28]. These mechanisms are depicted in Fig. 1(c) showing the CT scan slice of a specimen after tensile loading. To achieve this uncorrelated failure, CMCs normally have a sufficiently weak fiber–matrix interface or a porous matrix [29]. However, the optimum concept for composite microstructure is still a debatable topic, especially without understanding how crack propagation works.

For the experiments to obtain the training dataset, different types of samples were prepared here. Nextel 610 fibers (3 M Co, Maplewood, MN, USA) were used for all experiments. The fibers were heat cleaned at 600 °C for 2 h in a LHT 04/17 chamber furnace (Nabertherm GmbH, Lilienthal, Germany) to remove their polymeric coating, following the instructions of the supplier. Nextel 610 fiber bundles with 3000 denier were used for fiber characterization and for the fiber pullout tests. Single-filament and 10-filament samples were prepared by extracting individual fibers

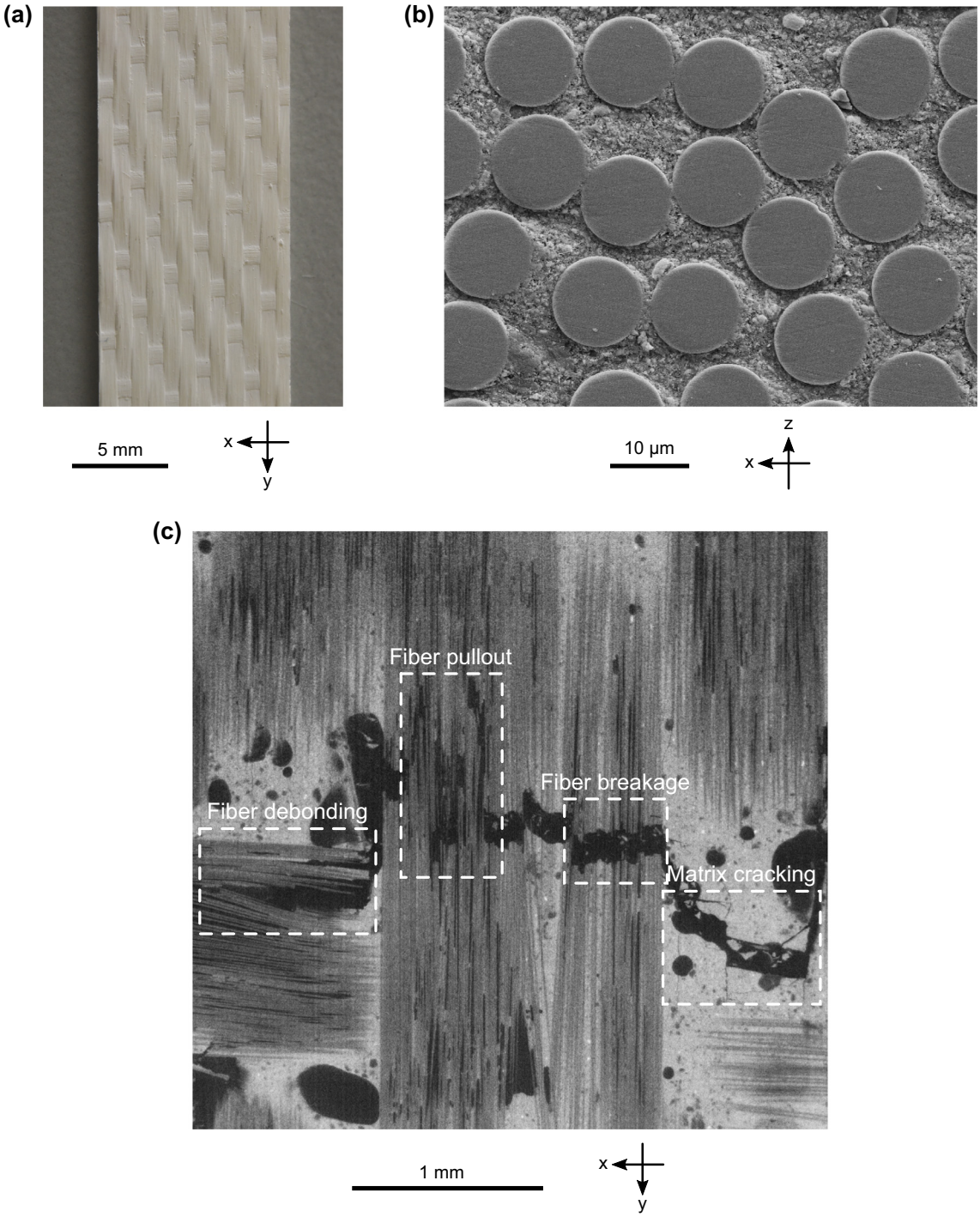

Fig. 1. Studied ceramic matrix composite with fiber reinforcement in × and y directions: (a) Photograph of CMC sample showing fiber pattern. (b) SEM micrograph of CMC sample showing cross-section of fibers in the y direction. (c) CT scan slice of CMC sample after tensile loading in the y direction. The matrix is the light gray phase, fibers are the dark gray phase and defects like pores and cracks are the black phase. From left to right, the following damage mechanisms can be observed: fiber debonding, fiber pullout, fiber breakage and matrix cracking.

from the bundle and gluing them to paper frames. For the fiber bundle test, the whole bundle containing approximately 750 fibers was used. Nextel 610 fiber fabrics DF-11 containing bundles with 1500 denier were used for the production of the composite samples.

The processing of the matrix for matrix characterization and composite production was done via the ionotropic gelation technique [30]. For that, a water-based slurry containing alginate chains as the binder was prepared. Two alginates were used in equal proportions: protanal LFR5/60 (FMC Corporation, Philadelphia, PA, USA) and alginic acid sodium salt from brown algae, medium viscosity (Sigma-Aldrich Chemie GmbH, Steinheim, Germany). The prepared slurry had a particle content of 50 vol%. Two alumina powders with different particle sizes were used: CT 1200 (d_{50} = 1200 nm; Almatis GmbH, Ludwigshafen, Germany) and TM-Dar (d_{50} = 200 nm; Taimei Chemicals, Tokyo, Japan). In

addition, 5-sulfosalicylic acid dihydrate ReagentPlus® (Sigma-Aldrich Chemie GmbH) was used as a dispersant. The suspension was prepared by combining the powders with double-deionized water, with pH adjusted to 9, under an ice bath with an overhead stirrer. Before using the slurry, aluminum acetate basic (Honeywell Specialty Chemicals Seelze GmbH, Seelze, Germany) was added to start the cross-link reaction, which slowly increases the viscosity of the suspension. Matrix samples were formed by casting the slurry into molds with the chosen geometry. For fiber pullout samples, the slurry was casted in a cylindrical mold and a fiber bundle was embedded 3 mm deep into the suspension. For the composite samples, the suspension was used to infiltrate the fiber fabrics. A total of 12 infiltrated fiber fabric layers were stacked together to achieve the desired sample height. All samples were dried in a climate chamber at room temperature and 80% of humidity for two days. Afterwards, the samples were sintered in the same chamber furnace at 1200 °C for 1 h. Sintering temperature and time were selected to obtain a porous matrix. Further details on the ionotropic gelation technique for the processing of Ox-CMCs can be seen in previous publications [30,31].

2.2. Mechanical tests

All experiments for the training dataset were performed with a universal testing machine Zwick Z005 (Zwick Roell Group, Ulm, Germany) using different testing setups. Fig. 2(a–e) show schematic representations of the experiments for the training dataset, while Table 1 lists specific details and expected outcomes of each test. The experiments can be divided into mechanisms related to matrix, fiber and fiber–matrix interface. Matrix samples were tested under 4-point bending test, following the standard DIN EN 843-1, to promote matrix crack initiation and propagation. In addition, notched samples were tested in the single-edge notch bending test (SENB) configuration following the standard DIN 51109. Having a notch as the "initial matrix crack", the objective of this test was to promote only matrix crack propagation. Both types of test were done with a loading speed of 0.5 mm/min. Fiber mechanisms were evaluated with three test configurations: single-filament (DIN EN 1007-4), 10-filaments and fiber bundle tensile tests (DIN EN 1007-5). While testing a single or 10 fibers promotes fiber breakage, it is possible to also measure the interaction between the fibers when testing a whole fiber bundle. Samples were tested with a loading speed of 0.1 mm/min. It should be highlighted that the matrix and fiber tests were done with two sets of dimensions (see Table 1) to evaluate the effect of sample dimension on the measured AE features.

As the name implies, fiber pullout was simulated by fiber pullout tests. For that, a special test setup was used. The cylindrical matrix with the embedded fiber bundle was attached to one end of the testing machine, while the free fiber bundle end was attached to the other end of the machine. These samples were tested in tension with a loading speed of 0.1 mm/min. Lastly, the produced composite plates were tested under short-beam bending (SBB) to promote interlaminar debonding. SBB tests were performed using a three-point bending test configuration with a support span (L_{SBB}) of 25 mm, following the standard DIN EN 658-5. The relatively short support span in relation to the sample height (h_{SBB}) was used to minimize the tensile/compressive stresses, while maximizing shear stresses to induce interlaminar failure. SBB tests were performed with a loading speed of 0.5 mm/min.

The characterization of the FW12 composite was done by tensile tests on a universal testing machine Zwick 1465 (Zwick Roell Group, Ulm, Germany). A laser extensometer PS-E50-0138-AM (Fiedler Optoelektronik GmbH, Lutzen, Germany) was used to measure strain contactless. Tests were conducted by applying the tensile load in one of the main fiber reinforcement directions (0°/90°) with a travelling speed of 1 mm/min following the standard DIN EN 658-1. A total of three samples with dog-bone geometry were loaded until failure for the main experiments (Fig. 2(f)). The dog-bone samples were cut from the same composite plate by laser cutting. Furthermore, a fourth sample with a reduced cross-section was tested for the ex-situ CT experiments. For that, circular notches with a radius of 7.5 mm were machined on a 180x20x3 mm^3 rectangular composite sample, resulting in a width of 3.2 mm in the middle of the sample. This sample was CT scanned before the tensile test. Then, the sample was loaded-unloaded with increments of 50 MPa for each loading cycle until 200 MPa. CT scans were made between each loading cycle. After the 200 MPa loading, the sample was loaded until failure and once more scanned.

2.3. Computer tomography scans

CT scans with resolution of 2.185 μm/voxel were performed with a Xradia 520 Versa X-ray microscope (ZEISS, Oberkochen, Germany). Scans were done with X-ray energy of 80 kV (7 W), 1600 projections per revolution and a 4x objective length. The scans before and after each loading–unloading cycle were matched by fiducial point-based image registration and by correcting rotational and translational differences. A non-local means filter was applied to the overlapping images to reduce the noise [32]. Since the contrast between the different phases of the composite was low, a deep learning model was applied for phase segmentation. A few slices of the scans were manually segmented into the following categories: matrix, fibers, pores, cracks in matrix region, cracks in fiber regions. This information was used to train a 3D U-net model and the validation dataset was used to evaluate their segmentation performance [33]. Training datasets were augmented with rotation, flip and ±10% scaling of original images. The 3D U-Net model was trained for 100 epochs. The training dataset was shuffled at every epoch to avoid overfitting. During the training process, the loss function decreased gradually and converged to a specific value. The initial learning rate reduced to 0.05 times to better convergence. The trained model was used to segment the remaining slices of the CT scans. An example of this automated segmentation can be seen in Fig. S1 of Supplementary data. Dragonfly software (version 2021.1, Object Research Systems (ORS) Inc.) was then used for 3D visualization and quantitative analysis of the segments. To account for the process-induced cracks and defects, crack volume before the loading was subtracted from the measured crack volume at each stage.

2.4. Acoustic emission monitoring

AE monitoring was performed during all mechanical tests. For the ex-situ CT test, AE monitoring was performed only during the loading–unloading cycles. The measurements were carried out with an AMSY4-PC system equipped with two VS600-Z2 sensors (Vallen Systeme GmbH, Icking, Germany). The sensors were glued to the samples or to the testing set-up using hot glue. The distance between the sensors for the tensile tests with ex-situ CT scans was of 50 mm, while the position of the sensors for the other tests can be seen Fig. 2(a–f). Before each test, the sensors were calibrated to estimate the AE velocity within the sample. This was done in order to later be able to localize the AE events by measuring the time of arrival difference between the sensors. Hence, only signals detected within the sample were considered for analysis, while the others were disregarded as background noise. Data acquisition was performed using gain of 34 dB, threshold of 30 dB, duration discrimination time of 50 μs and rearm time of 100 μs.

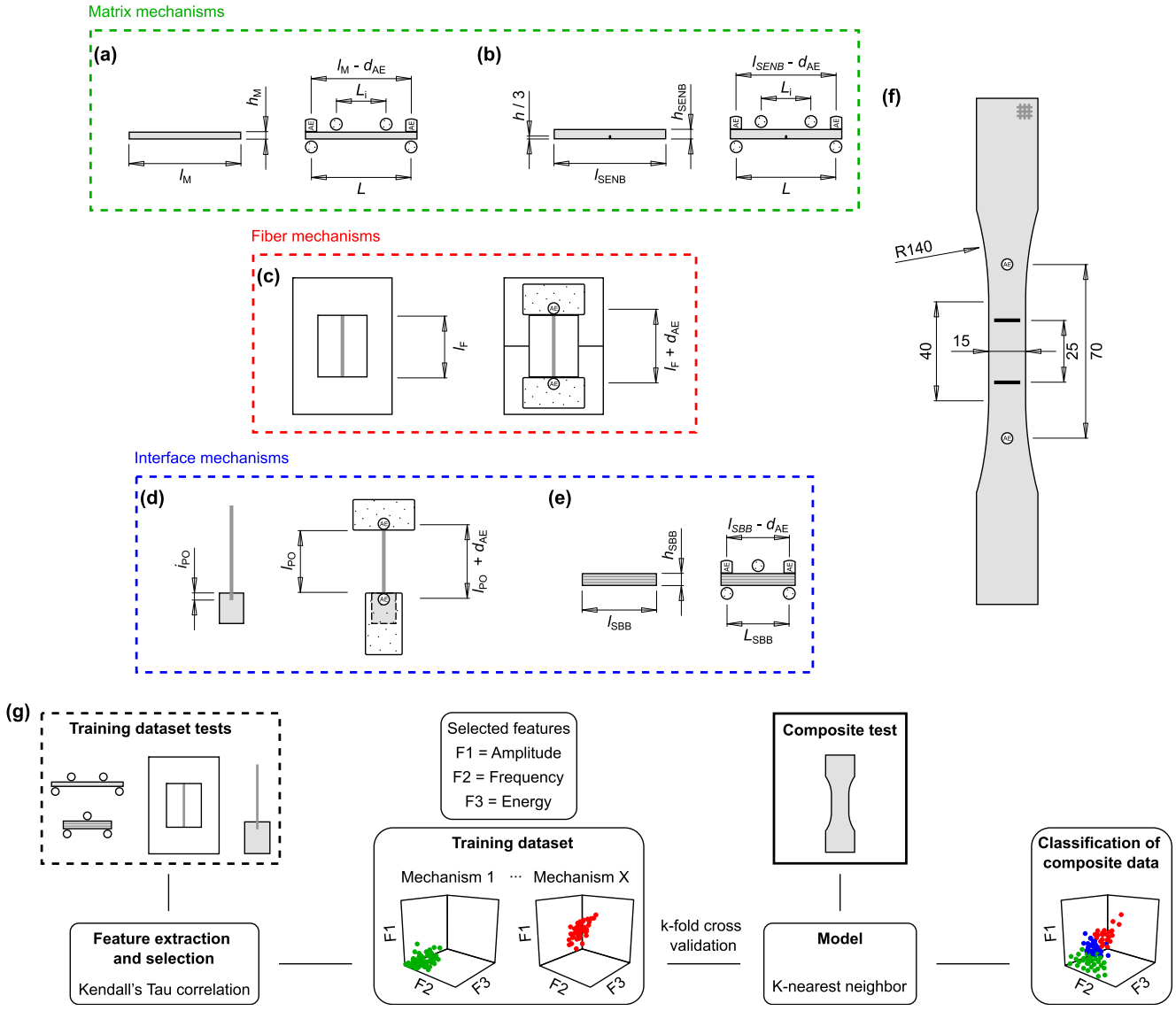

Fig. 2. Testing set-up and machine learning model: (a-e), Samples (left) and set-ups (right) of experiments for training dataset highlighting the position of the AE sensors (d_{AE} = 4.75 mm): matrix bending test (a), matrix single-edge notch bending test (b), fiber single-filament, 10-filament and bundle tensile test (c), fiber pullout tensile test (d), composite short-beam bending test (e). Test dimensions are given in Table 1. (f) Composite tensile test, in which the load is applied in the same direction as one of the fiber axes. (g) Flow chart representation of supervised pattern recognition method for AE data analysis.

2.5. Supervised classification approach

Fig. 2(a) illustrates the used approach for the supervised classification of AE signals. The first step is to obtain labeled inputs to be used as a training dataset. For that, the aforementioned training dataset tests were performed, in which the different damage mechanisms are simulated. Feature extraction was done using the Vallen AE-Suite software (Vallen Systeme GmbH, Icking, Germany). The following features were recorded: maximum amplitude, total hit duration, rise time until maximum amplitude, number of threshold crossings, hit energy (1 eu = 10^{-18} J), average frequency and event linear location. The data acquired during the aforementioned tests is then used to compose the training dataset. To select the appropriate AE features for the analysis, a correlation matrix based on Kendall's Tau correlation [34] is used. The idea is to identify which features have the highest correlation with the identified damage mechanisms. To avoid bias or overfitting, features that are highly correlated with each other are discarded for training the model. As a result, maximum amplitude, average frequency and energy were selected as input features.

The classification model was implemented in Python using the following libraries: *sklearn*, *pandas* and *numpy*. Data input (training dataset and data to be classified) were scaled using the MinMaxScaler function in python, so that all features present values between 0 and 1. The classification algorithm used in this work is the k-nearest neighbor (KNN) [35], in which the Euclidean distance between the data is used to classify a signal to a specific class. Due to the nature of the KNN algorithm, time complexity and space complexity are relatively larger if compared to other clustering algorithms. Because of that, it can be computationally expensive. Nevertheless, KNN was chosen since it is a well-established and easy-to-use algorithm for such multivariate analysis [14]. Other algorithms such as random forest, SGD, and naive bayes were tested but showed lower accuracy and, therefore, were not continued in this work. The number of neighbors (k) is selected considering the size of the dataset and misclassification error. For

Table 1
Experiments performed to collect data for training dataset and expected damage mechanisms.

Test	# of samples per geometry	Dimensions	Expected mechanisms
Matrix bending test	30	l_M = 45 and 70 mm, h_M = 4 and 6 mm, L_i = 20 mm L = 40 and 60 mm	Matrix crack initiation and propagation
Matrix single edge notch bending test	20	l_{SENB} = 45 and 70 mm, h_{SENB} = 4 and 6 mm, L_i = 20 mm L = 40 and 60 mm	Matrix crack propagation
Fiber single-filament tensile test	25	l_F = 25 and 70 mm	Fiber breakage
Fiber 10-filament tensile test	5	l_F = 70 mm	Fiber breakage
Fiber bundle tensile test	5	l_F = 25 and 70 mm	Fiber breakage + fiber interactions
Fiber pullout	14	l_{PO} = 25 mm i_{PO} = 3 mm	Fiber pullout + fiber breakage
Composite short-beam bending test	10	l_{SBB} = 30 mm, h_{SBB} = 5.0 ± 0.1 mm, L_{SBB} = 25 mm	Interlaminar debonding + matrix and fiber breakage

that, the number of "k" was varied and the optimal value was chosen as the value with the lowest misclassification. To obtain a reliable prediction model, testing its accuracy is especially important. K-fold cross validation was used for this purpose. In short, the training dataset is randomly shuffled and divided into k groups. Each data group is evaluated individually using the remaining groups as the training dataset. Since the procedure only uses data that is already known, the model evaluation scores can be calculated. The trained model is then capable of classifying previously unknown data using what it learnt from the training dataset. The input data to be analyzed was collected during tensile tests of the studied commercial CMC (Fig. 2(g)).

3. Results and discussion

3.1. Training dataset

Fig. 3 illustrates the data acquired during the experiments for the training dataset. For better visualization of the data, the graphs show the amplitude and frequency of the signals measured during the respective tests. Nevertheless, energy was also used for the classification. Most signals from matrix tests are in the range of 33–55 dB of amplitude and 0.05–0.40 MHz of frequency (Fig. 3(a)). Although bending and SENB tests were designed for different purposes (see Table 1), the measured signals are very similar in terms of amplitude and frequency. However, SENB signals have slightly lower energy (see Table S1 of Supplementary data). This may be related to the smaller load-bearing cross-section of notched samples and shorter crack path, not to mention that the notch promotes matrix cracking more easily. Sample dimension did not seem to have a significant effect on the measured features; although it is known that AE features can be influenced by sample geometry as they are dependent on the time of arrival at the sensor [36]. It can be presumed that the signal attenuation is low within the used ranges, but may differ with different geometries. Hence, all signals collected during these tests were labeled as "matrix cracking" for the training dataset.

Fiber breakage signals of single-filament and 10-filament tensile tests are in the range of 65–90 dB of amplitude and 0.30–0.50 MHz of frequency (Fig. 3(b)), i.e., a much different range than matrix cracking signals (Fig. 3(a)). Nevertheless, different signals are measured when testing a fiber bundle (Fig. 3(c)). It is clear that most signals belong to fiber breakage, but signals with lower amplitude and high dispersion of frequency are measured as well. These low-amplitude signals are considered to be generated by the interactions between broken fibers during loading. As the fibers of the bundle start to fail, friction between the newly broken fibers can generate signals with high dispersion and generally low energy. This may be related to the fact that friction will depend on the random relative movement of the different surfaces. Therefore, signals measured during fiber bundle tests were manually labeled as "fiber breakage" or "friction" by comparing with the previously identified fiber breakage signals of Fig. 3(b). Furthermore, fiber length did not seem to influence the measured AE features, just like in the matrix tests.

Interface characterization is more complex than the previously described tests as it depends on the interaction between fibers and matrix, which may also fail during loading. Therefore, these tests were performed after obtaining information about fiber and matrix AE signatures. During fiber pullout tests, the loading can cause not only pullout, but also fiber breakage. In order to filter out the fiber breakage signals, only signals localized in the fiber–matrix embedded region were evaluated, which are displayed in Fig. 3(d). It is interesting to see that the range of amplitude and frequency of these signals lay somewhat between the signals of matrix (Fig. 3(a)) and fibers (Fig. 3(b)). Lastly, interlaminar debonding was measured by composite SBB test. Although this test configuration is planned to promote interlaminar failure, matrix and fiber breakage can also take place due to the applied tensile/compressive stresses. Hence, all types of AE signals can be measured, as depicted for one example test in Fig. 3(e). In general, AE signals with low amplitude can be attributed to matrix cracking, which can occur throughout the test. As interface debonding starts to take place, exposed fibers can also break, albeit less frequently, generating high-energy AE signals. Hence, labeling of interface debonding signals was done manually by comparing with matrix (Fig. 3(a)) and fiber signals (Fig. 3(b)), as well as with the literature. It can be seen that there is a considerable amount of signals between the ranges of matrix and fiber signals. Other authors have also related interface damage to the range of 55–65 dB [37].

After properly labeling all signals with their respective damage sources, the training dataset is built. Average amplitude and frequency of the identified mechanisms are given in Fig. 3(f). Most mechanisms have a rather distinct range, which can be associated with the properties of the individual constituents. For instance, the matrix is considered the weakest component of a composite. Hence, matrix signals have low amplitude and energy. Debonding and pullout show similar features since both are originated from interface failure. Their main difference lies on the measured AE energy (Table S2 of Supplementary data). It can be concluded that it is easier to promote debonding, in which cracks propagate also through the weak matrix, than to pull a fiber out, which also involves friction. The precision, recall and F1-score of each damage mode measured by K-fold cross validation are shown in Table S3 of Supplementary data. Because of similarities between some of the damage modes, their precision was affected. Still, the model accuracy, in terms of average K-fold score, was measured to be equal to 88%.

3.2. AE event classification of composite tensile tests

Fig. 4(a) shows the classification of AE signals collected during the tensile test of the commercial composite. It is clear that the

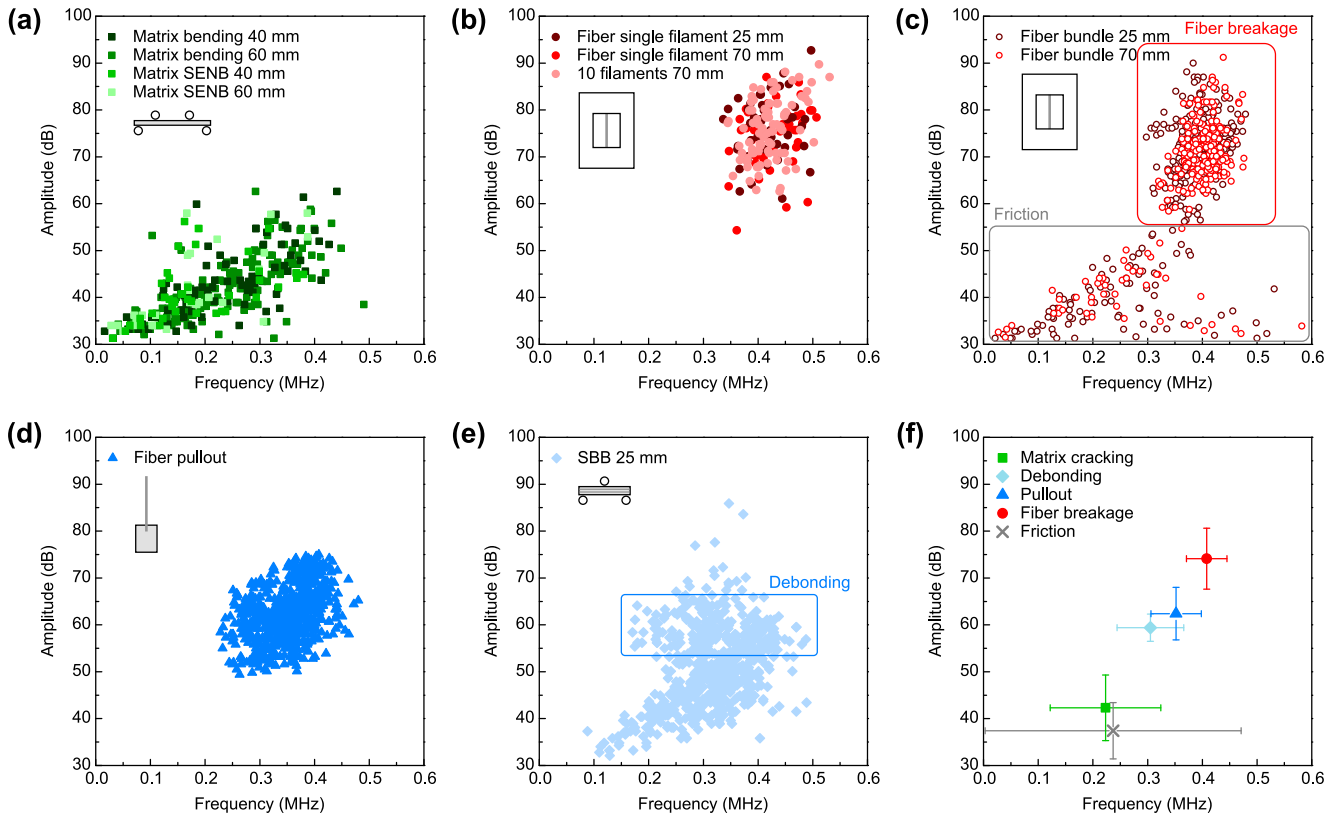

Fig. 3. AE signals collected during experiments for training dataset: (a) Matrix bending tests. (b) Fiber single-filament and 10-fialment tests. (c) Fiber bundle tensile test. (d) Fiber pullout tensile tests. (e) Composite short-beam bending test. (f) Average features of measured mechanisms.

model output corresponds very well with the previously observed ranges of each damage mechanism (Fig. 3). By identifying the damage source, it is possible to investigate and quantify the damage development during loading, providing crucial information about the mechanical behavior of the studied material. Fig. 4(b) shows the stress–strain diagram of the same sample, along with the cumulative AE hit count divided into the five different classes. The presented stress–strain curve is very typical for porous CMCs being loaded along one of the fiber axes, in which a small degree of non-linearity is observed [27]. As both matrix and fibers are essentially brittle, the non-linear deformation is mainly associated with the damage development along matrix, interface and fibers. AE activity starts to increase at around 50 MPa. Most of the initial signals are classified as either matrix cracking or debonding. As aforementioned, the matrix is the weakest component of the composite. Hence, cracks are much easier to start and propagate along the matrix porosity, which alleviates the stress concentrations on the fibers. Similarly, the porosity at the fiber–matrix interface can facilitate debonding. It is interesting that even at low stresses, signals associated with fiber breakage are observed, although the fibers are presumably much stronger. In general, ceramic fibers in a bundle can have a high dispersion of strength values since each fiber can have different microstructural defects [38]. Hence, the weaker fibers can fail at lower stresses. Nevertheless, the increase of fiber breakage AE hits is much slower than for matrix and debonding, i.e., cracks propagate preferably through matrix and interface as they offer "less resistance". As loading progresses, signals associated with fiber pullout and friction start being detected as well. This indicates that pullout can only happen after a certain amount of fibers have broken, while friction signals are mostly associated with the relative movement of internal surfaces as the different constituents fail. At the maximum stress, a signal with much higher energy and duration is detected. It is expected that this signal is caused by multiple failure modes happening simultaneously, mainly dominated by fibers breakage. Therefore, this high-energy signal was not considered in the analysis and is not shown in Fig. 4.

More information is obtained with the quantification of the total hit count and total AE energy of the classified signals (Fig. 4 (c)). For instance, although matrix cracking is the most frequent mechanism, it corresponds to about only 10% of the total measured AE energy. To understand the significance of the AE energy, one should recall that AE signals are generated due to microstructural changes. When cracking occurs, part of the mechanical energy dissipates in different forms such as acoustic emission, heat, the formation of internal surfaces, etc. Therefore, AE energy can give an indication of the dissipated mechanical energy of each mechanism. In this sense, the energy sum of fiber breakage signals is much higher than other mechanisms, even though they are only 10% of the total hit count. Since fibers are the main load-bearing components of a composite, it would be ideal to have more dissipation of energy by matrix cracking and interface debonding as these are crack-deflection mechanisms. For this commercial composite, they represent together about 40% of the total measured AE energy. Therefore, in order to improve damage tolerance, one could increase the matrix porosity or adjust the fiber–matrix interface to promote more matrix cracking or interface debonding, respectively. Friction can also potentially help on energy dissipation. However, the contribution of this mechanism is rather small during quasi-static loading. Still, it could play a bigger role for dynamic loadings.

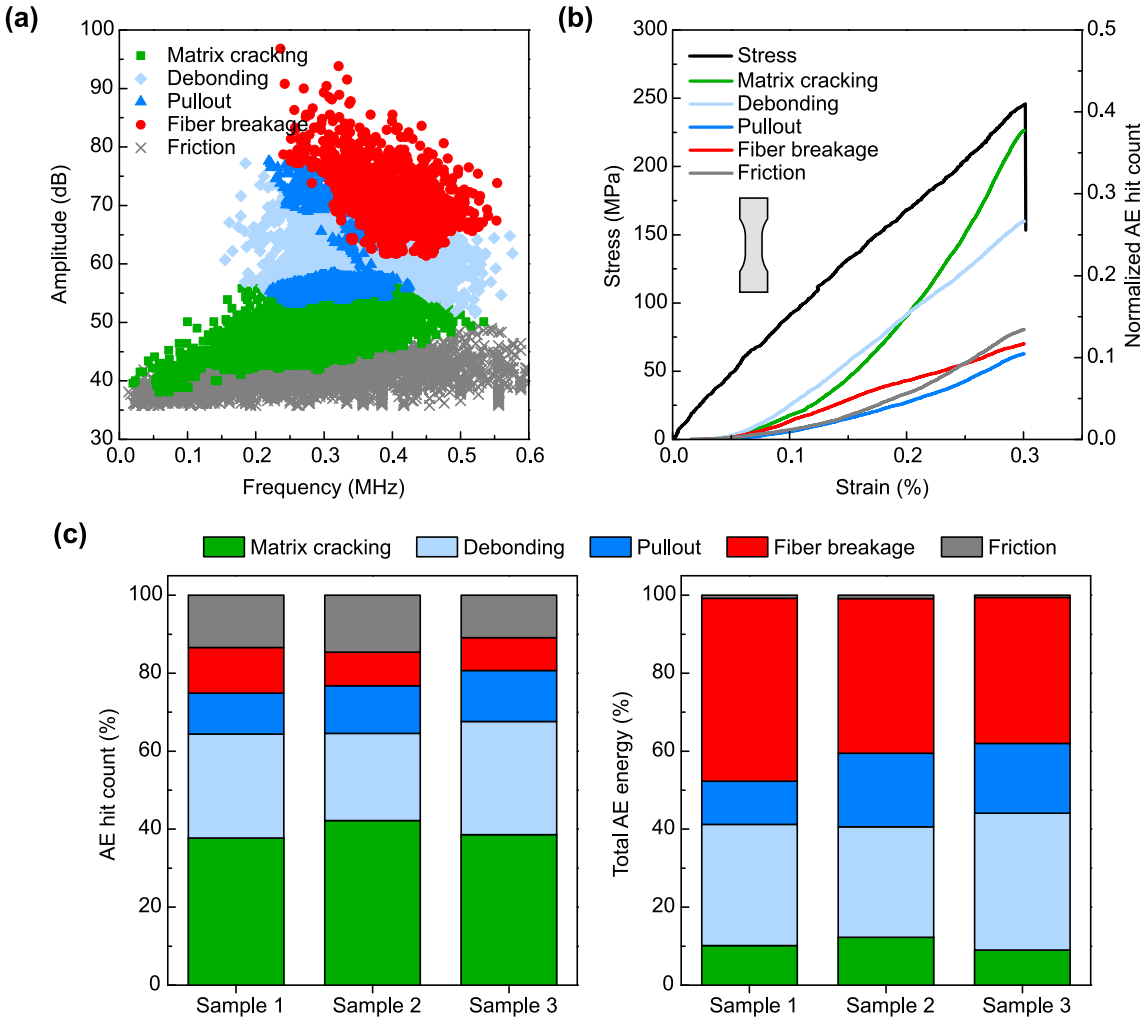

Fig. 4. Composite tensile test: (a) Classified AE signals collected during tensile test of a commercial composite sample. (b) Stress–strain curve and cumulative AE hit count of the same sample. AE hit count was normalized in relation to the total amount of measured AE hits during the test. (c) Quantification of classified AE signals hit count and energy of all three tested composite samples.

3.3. Ex-situ X-ray computer tomography

One additional test was conducted to compare the information acquired by AE analysis with the quantification of cracks by ex-situ CT. To ensure that the damage would occur on the scanned area, the sample had a reduced section as schematized in Fig. 5(a). Most of the measured signals are from the reduced section since the stress is higher there. Nevertheless, AE signals were measured slightingly outside of the scanned region during the last loading until failure as well. To properly correlate the measured AE signals with the performed ex-situ CT scans, only the signals localized within the scanned volume were analyzed. Fig. 5(b) shows the stress–strain and cumulative AE hit count of this test. In general, this sample shows a similar tendency as the previous samples. Still, fiber pullout signals occur earlier for this specimen, which may be related to the fact that loading–unloading can promote interface damage.

Phase segmentation of the CT scans was performed to locate and quantify the crack patterns. Cracks were grouped as either in the matrix region (matrix cracking) or in the fiber region (debonding, pullout or fiber breakage). The segmented cracks before the loading and after failure are displayed in Fig. 5(c). Even before loading, the composite already presents microstructural defects besides matrix porosity. Such defects are rather common in this type of material due to its processing, in which the matrix densification is restricted by the dense fibers [39]. This mismatch causes thermal stresses that can lead to the formation of cracks. Therefore, the amount of cracks generated during loading was calculated by subtracting the amount of initial cracks (Fig. 5(d)). In the literature, different authors have tried to relate the information of crack imagining with AE quantification [22,40]. This correlation can be rather difficult as the crack volume will depend not only on the frequency and intensity of damage, but also on how the cracks initiate and propagate along each constituent. For instance, fiber breakage results in high-energy signals due to their higher stiffness, but the generated crack volume is relatively small. Furthermore, the residual thermal stresses can facilitate initial cracking, which generates low-energy AE signals. This can be seen when comparing the AE activity and the generated matrix crack volume up to the loading of 100 MPa. Although there is a considerable increase of crack volume (Fig. 5(d)), there is still very little AE activity up to 100 MPa (Fig. 5(b)). After this initial cracking however, both techniques show similar tendencies. Considering only the matrix crack volume generated after 100 MPa, 4.7% occurs up to 150 MPa, while 23.9% takes place up to 200 MPa. Comparably considering only matrix cracking AE hits after the 100 MPa loading, 5.1% of the total measured AE energy happens up to 150 MPa, while 21.3% occurs up to

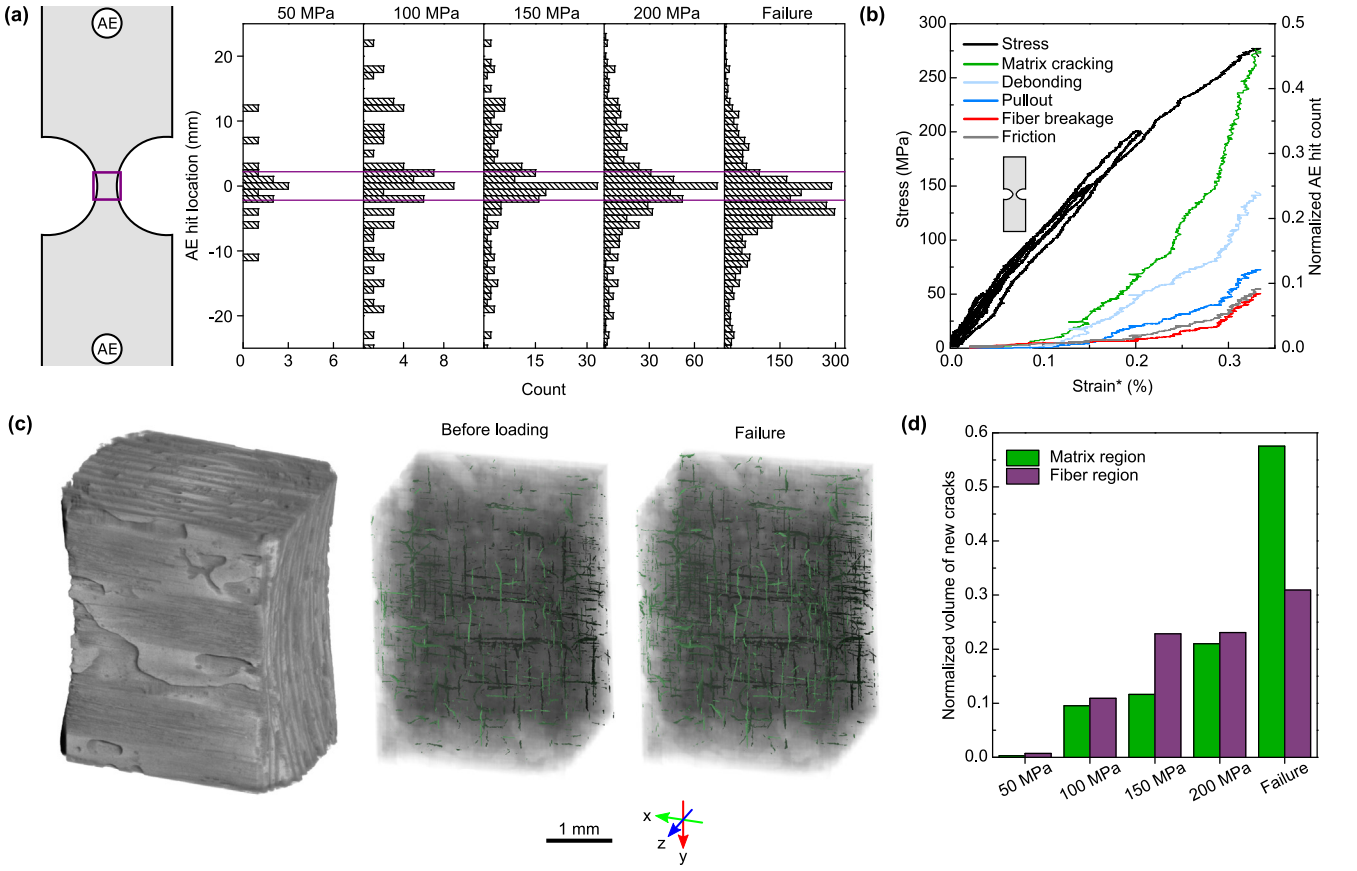

Fig. 5. Composite tensile test with unloading cycles for ex-situ CT scans: (a) Sample geometry and localization of collected AE signals. (b) Stress–strain curve and cumulative AE hit count. The strain was measured outside the reduced cross-section. AE hit count was normalized in relation to the total amount of measured AE hits during the test and only signals detected in the scanned volume (purple box of (a)) were considered. (c) Segmentation of cracks measured by CT of composite before loading and after failure. (d) Quantification of crack volume generated during loading–unloading cycles in relation to crack volume before loading. Crack volume of new cracks was normalized in relation to the initial crack volume of the respective region. (For interpretation of the references to colour in this figure legend, the reader is referred to the web version of this article.)

200 MPa. This indicates that both techniques are somewhat in agreement.

4. Conclusions

In summary, a method for the classification of AE signals based on supervised machine learning is presented in this work. Experiments were designed to obtain a reliable training dataset for the supervised classification model. The collected training dataset contains key details about the different breaking behaviors of fibers and matrices, as well as their interface. This allows for the correct identification of AE signals, giving essential information on the location, time, frequency and intensity of each damage mechanism. Not only such analysis helps us understand damage development during loading, but also helps us see which mechanisms have a higher contribution on crack propagation and energy dissipation. This is very important for the further development of composites like CMCs. Furthermore, the presented methodology can also be applied to study different complex and multi-phase materials. Adapting the experiments for the training dataset to consider damage mechanisms of other types of composites and materials would be the next step to build a library containing characteristic AE features. In addition, other in-situ analysis techniques can be applied in tandem, but it should still be highlighted that they give different information and should be used to complement each other. For instance, CT scans can give information on the crack patterns and total crack volume, but their detection resolution is smaller and time dependent.

Data availability

The collected training dataset is available in Mendeley Data (https://doi.org/10.17632/svz439j8hb.1). Other data supporting the findings of this study are available in the article and its Supplementary information.

Declaration of Competing Interest

The authors declare that they have no known competing financial interests or personal relationships that could have appeared to influence the work reported in this paper.

Acknowledgements

The authors would like to thank W.E.C. Pritzkow from the company Pritzkow Spezialkeramik for providing the composite samples studied in this work. The authors also express their gratitude to J. Horvath for the CT scans, as well as for A. Michna for the help with the mechanical tests. This research did not receive any specific grant from funding agencies in the public, commercial, or not-for-profit sectors.

Appendix A. Supplementary material

Supplementary data to this article can be found online at https://doi.org/10.1016/j.matdes.2023.111745.

References

[1] A. Kelly, C. Zweben, Comprehensive Composite Materials, Pergamon, Oxford, United Kingdom, 2000.
[2] R.S. Ambekar, B. Kushwaha, P. Sharma, F. Bosia, M. Fraldi, N.M. Pugno, C.S. Tiwary, Topologically engineered 3D printed architectures with superior mechanical strength, Mater. Today 48 (2021) 72–94.
[3] S. Bhadra, M. Rahaman, P. Noorunnisa Khanam, Electrical and electronic application of polymer-carbon composites, in: M. Rahaman, D. Khastgir, A.K. Aldalbahi (Eds.), Carbon-Containing Polymer Composites, Springer, Singapore, Singapore, 2019, pp. 397–455.
[4] P.S. Owuor, V. Chaudhary, C.F. Woellner, V. Sharma, R.V. Ramanujan, A.S. Stender, M. Soto, S. Ozden, E.V. Barrera, R. Vajtai, D.S. Galvão, J. Lou, C.S. Tiwary, P.M. Ajayan, High stiffness polymer composite with tunable transparency, Mater. Today 21 (5) (2018) 475–482.
[5] J.P. Forna-Kreutzer, J. Ell, H. Barnard, T.J. Pirzada, R.O. Ritchie, D. Liu, Full-field characterisation of oxide-oxide ceramic-matrix composites using X-ray computed micro-tomography and digital volume correlation under load at high temperatures, Mater. Des. 208 (2021) 109899.
[6] Z. Quiney, E. Weston, P. Ian Nicholson, S. Pattison, M.R. Bache, Volumetric assessment of fatigue damage in a SiCf/SiC ceramic matrix composite via in situ X-ray computed tomography, J. Eur. Ceram. Soc. 40 (11) (2020) 3788–3794.
[7] M.R. Bache, C.D. Newton, J.P. Jones, S. Pattison, L. Gale, P.I. Nicholson, E. Weston, Advances in damage monitoring techniques for the detection of failure in SiCf/SiC ceramic matrix composites, Ceramics 2 (2) (2019) 347–371.
[8] K.G. Dassios, E.Z. Kordatos, D.G. Aggelis, T.E. Matikas, Crack growth monitoring in ceramic matrix composites by combined infrared thermography and acoustic emission, J. Am. Ceram. Soc. 97 (1) (2014) 251–257.
[9] V. Mazars, O. Caty, G. Couégnat, A. Bouterf, S. Roux, S. Denneulin, J. Pailhès, G.L. Vignoles, Damage investigation and modeling of 3D woven ceramic matrix composites from X-ray tomography in-situ tensile tests, Acta Mater. 140 (2017) 130–139.
[10] Y. Chen, L. Gélébart, C. Chateau, M. Bornert, A. King, P. Aimedieu, C. Sauder, 3D detection and quantitative characterization of cracks in a ceramic matrix composite tube using X-ray computed tomography, Exp. Mech. 60 (3) (2020) 409–424.
[11] G.N. Morscher, R. Maxwell, Monitoring tensile fatigue crack growth and fiber failure around a notch in laminate SIC/SIC composites utilizing acoustic emission, electrical resistance, and digital image correlation, J. Eur. Ceram. Soc. 39 (2) (2019) 229–239.
[12] C. Liu, Y. Chen, D. Shi, J. Marrow, X. Jing, X. Yang, In situ investigation of failure in 3D braided SiCf/SiC composites under flexural loading, Compos. Struct. 270 (2021) 114067.
[13] M. Roth, E. Mojaev, E. Dul'kin, P. Gemeiner, B. Dkhil, Phase transition at a nanometer scale detected by acoustic emission within the cubic phase Pb(Zn1/3Nb2/3)O3−xPbTiO3 relaxor ferroelectrics, Phys. Rev. Lett. 98(26) (2007) 265701.
[14] C. Muir, B. Swaminathan, A.S. Almansour, K. Sevener, C. Smith, M. Presby, J.D. Kiser, T.M. Pollock, S. Daly, Damage mechanism identification in composites via machine learning and acoustic emission, NPJ Comput. Mater. 7 (1) (2021) 95.
[15] N. Godin, P. Reynaud, G. Fantozzi, Challenges and limitations in the identification of acoustic emission signature of damage mechanisms in composites materials, Appl. Sci. 8 (8) (2018) 1267.
[16] N. Guel, Z. Hamam, N. Godin, P. Reynaud, O. Caty, F. Bouillon, A. Paillassa, Data merging of AE sensors with different frequency resolution for the detection and identification of damage in oxide-based ceramic matrix composites, Materials 13 (20) (2020) 4691.
[17] R. Gutkin, C.J. Green, S. Vangrattanachai, S.T. Pinho, P. Robinson, P.T. Curtis, On acoustic emission for failure investigation in CFRP: pattern recognition and peak frequency analyses, Mech. Syst. Sig. Process. 25 (4) (2011) 1393–1407.
[18] A. Sibil, N. Godin, M. R'Mili, E. Maillet, G. Fantozzi, Optimization of acoustic emission data clustering by a genetic algorithm method, J. Nondestr. Eval. 31 (2) (2012) 169–180.
[19] A.K. Das, D. Suthar, C.K.Y. Leung, Machine learning based crack mode classification from unlabeled acoustic emission waveform features, Cem. Concr. Res. 121 (2019) 42–57.
[20] W. Zhou, R. Qin, K.-N. Han, Z.-Y. Wei, L.-H. Ma, Progressive damage visualization and tensile failure analysis of three-dimensional braided composites by acoustic emission and micro-CT, Polym. Test. 93 (2021) 106881.
[21] S. Momon, N. Godin, P. Reynaud, M. R'Mili, G. Fantozzi, Unsupervised and supervised classification of AE data collected during fatigue test on CMC at high temperature, Compos. A Appl. Sci. Manuf. 43 (2) (2012) 254–260.
[22] E. Maillet, A. Singhal, A. Hilmas, Y. Gao, Y. Zhou, G. Henson, G. Wilson, Combining in-situ synchrotron X-ray microtomography and acoustic emission to characterize damage evolution in ceramic matrix composites, J. Eur. Ceram. Soc. 39 (13) (2019) 3546–3556.
[23] M.G.R. Sause, S. Horn, Simulation of acoustic emission in planar carbon fiber reinforced plastic specimens, J. Nondestr. Eval. 29 (2) (2010) 123–142.
[24] M.Y. Bhuiyan, J. Bao, B. Poddar, V. Giurgiutiu, Toward identifying crack-length-related resonances in acoustic emission waveforms for structural health monitoring applications, Struct. Health Monit. 17 (3) (2017) 577–585.
[25] M. Saeedifar, M.N. Saleh, S.T. De Freitas, D. Zarouchas, Damage characterization of adhesively-bonded Bi-material joints using acoustic emission, Compos. B Eng. 176 (2019) 107356.
[26] W.E.C. Pritzkow, R.S.M. Almeida, L.B. Mateus, K. Tushtev, K. Rezwan, All-oxide ceramic matrix composites (OCMC) based on low cost 3M Nextel™ 610 fabrics, J. Eur. Ceram. Soc. 41 (5) (2021) 3177–3187.
[27] K. Tushtev, R.S.M. Almeida, Oxide/oxide CMCs – porous matrix composite systems; composites with interface coatings, in: P.W.R. Beaumont, C.H. Zweben (Eds.), Comprehensive Composite Materials II, Elsevier, Oxford, 2018, pp. 130–157.
[28] F.W. Zok, Developments in oxide fiber composites, J. Am. Ceram. Soc. 89 (11) (2006) 3309–3324.
[29] D. Koch, K. Tushtev, G. Grathwohl, Ceramic fiber composites: experimental analysis and modeling of mechanical properties, Compos. Sci. Technol. 68 (5) (2008) 1165–1172.
[30] R.S.M. Almeida, T.F.S. Pereira, K. Tushtev, K. Rezwan, Obtaining complex-shaped oxide ceramic composites via ionotropic gelation, J. Am. Ceram. Soc. 102 (1) (2019) 53–57.
[31] R.S.M. Almeida, H. Farhandi, K. Tushtev, K. Rezwan, Joining oxide ceramic matrix composites by ionotropic gelation, Int. J. Appl. Ceram. Technol. 17 (4) (2020) 1574–1581.
[32] A. Buades, B. Coll, J.M. Morel, A non-local algorithm for image denoising, in: 2005 IEEE Computer Society Conference on Computer Vision and Pattern Recognition (CVPR'05), vol. 2, 2005, pp. 60–65.
[33] Ö. Çiçek, A. Abdulkadir, S.S. Lienkamp, T. Brox, O. Ronneberger, 3D U-Net: learning dense volumetric segmentation from sparse annotation, in: S. Ourselin, L. Joskowicz, M.R. Sabuncu, G. Unal, W. Wells (Eds.), Medical Image Computing and Computer-Assisted Intervention – MICCAI 2016, Springer International Publishing, Cham, 2016, pp. 424–432.
[34] M.G. Kendall, A new measure of rank correlation, Biometrika 30 (1/2) (1938) 81–93.
[35] F. Pedregosa, G. Varoquaux, A. Gramfort, V. Michel, B. Thirion, O. Grisel, M. Blondel, P. Prettenhofer, R. Weiss, V. Dubourg, Scikit-learn: machine learning in Python, J. Mach. Learn. Res. 12 (2011) 2825–2830.
[36] G.N. Morscher, N. Godin, Use of acoustic emission for ceramic matrix composites, Ceram. Matrix Compos. (2014) 569–590.
[37] S. Gholizadeh, Z. Leman, B.T.H.T. Baharudin, O. Inayatullah, Acoustic emission analysis for characterisation of damage mechanisms in glass fiber reinforced polyester composite, Aust. J. Mech. Eng. 16 (1) (2018) 11–20.
[38] D. Wilson, Statistical tensile strength of Nextel™ 610 and Nextel™ 720 fibres, J. Mater. Sci. 32 (10) (1997) 2535–2542.
[39] P.O. Guglielmi, D. Blaese, M.P. Hablitzel, G.F. Nunes, V.R. Lauth, D. Hotza, H.A. Al-Qureshi, R. Janssen, Microstructure and flexural properties of multilayered fiber-reinforced oxide composites fabricated by a novel lamination route, Ceram. Int. 41 (6) (2015) 7836–7846.
[40] G.N. Morscher, Stress-dependent matrix cracking in 2D woven SiC-fiber reinforced melt-infiltrated SiC matrix composites, Compos. Sci. Technol. 64 (9) (2004) 1311–1319.